Solar Energy 228 (2021) 531–539

Contents lists available at ScienceDirect

Solar Energy

journal homepage: www.elsevier.com/locate/solener

A novel passivating electron contact for high-performance silicon solar cells by ALD Al-doped TiO_2

Ying Liu [a,1], Borong Sang [b,1], Md. Anower Hossain [b], Kun Gao [a], Hao Cheng [a], Xiaomin Song [a], Sihua Zhong [a], Linxing Shi [a], Wenzhong Shen [c], Bram Hoex [b,*], Zengguang Huang [a,*]

[a] School of Science, Jiangsu Ocean University, Lianyungang 222005, Jiangsu Province, PR China
[b] School of Photovoltaic and Renewable Energy Engineering, UNSW, Sydney, New South Wales 2052, Australia
[c] School of Physics and Astronomy, Key Laboratory of Artificial Structures and Quantum Control (Ministry of Education), Shanghai Jiao Tong University, Shanghai 200240, PR China

ARTICLE INFO

Keywords:
Passivated contact
Atomic layer deposition
Passivation
Conductivity
High-performance solar cells

ABSTRACT

Titanium oxide (TiO_2) thin film has attracted wide interest in high-efficiency silicon solar cells as an electron selective contact due to its low conduction band offset with silicon and an excellent level of passivation, while the incorporation of a small amount of dopants is also expected to improve the performance of thin films. In this work, assisted with density functional theory (DFT) modelling, we study the electronic band structure of aluminum (Al)-doped TiO_2 (ATO). The atomic-layer-deposited (ALD) ATO thin films are successfully prepared, and the elemental analysis, passivation effect, thermal stability, conductivity and optical properties of the ATO are systematically investigated. An ultra-high effective minority carrier lifetime (τ_{eff}) of 1.9 ms and a low contact resistivity (ρ_c) of 0.1 $\Omega{\cdot}cm^2$ are simultaneously achieved on silicon wafers. Meanwhile, it is found that the ATO thin films possess better thermal stability than the TiO_2 thin film. Finally, a large-area (118.7 × 100 mm^2) *p*-type passivated emitter and rear contact (PERC) solar cells integrated with an ALD ATO layer on the illumination side was fabricated, and a champion efficiency of 21.4% was achieved with an optimal Al concentration in ATO, which is significantly higher than a PERC solar cell with intrinsic TiO_2. This work shows ATO a very attractive alternative achieving high-efficiency crystalline silicon solar cells.

1. Introduction

Carrier selective contacts (CSCs), which collect and transport one type of carrier (electron or hole) from the silicon absorber and simultaneously provide excellent passivation of a crystalline silicon (c-Si) surface are extensively studied to increase the energy conversion efficiency of c-Si solar cells (Matsui et al., 2020; Yu et al., 2018). The nature of CSCs is the strong asymmetry in carrier conductivity which can be achieved in various ways. The most common method is using highly doped silicon in combination with an interface passivation layer that is sufficiently thin to allow for majority carrier transport. In a tunnel oxide passivated contact (TOPCon) device structure, an ultra-thin tunnelling silicon dioxide (SiO_2) layer is combined with a doped polycrystalline silicon layer (Feldmann et al., 2014). In silicon heterojunction (SHJ) solar cells, a thin intrinsic and phosphorus/boron-doped amorphous silicon (a-Si: H) is used (Tanaka et al., 1992). However, TOPCon contacts still have some Auger recombination (resulting from the diffusion of dopants into the underlying silicon substrate), and both TOPCon and SHJ suffer from parasitic photon absorption (Yang et al., 2016a; Zhang et al., 2018). An alternative way to achieve carrier-selectivity is to exploit asymmetric band-alignment with c-Si or use materials with a relatively high or low work function compared to c-Si. Several transition metal oxides (TMOs) (Tyagi et al., 2019) have these desirable properties in addition to excellent electronic properties, negligible parasitic absorption, and a low cost and simple deposition process at relatively modest substrate temperatures.

Sub-stoichiometric titanium oxide (TiO_x) has demonstrated excellent performance as electron-selective passivating contact on c-Si (Nagamatsu et al., 2015; Yang et al., 2016a, 2016b), which is attributed to the asymmetric current flow at the c-Si/TiO_x interface with a small conduction band offset and a large valence band offset. Bullock et al. (2019) fabricated a partial hetero-contact for c-Si solar cells, which achieved an

* Corresponding authors.
E-mail addresses: b.hoex@unsw.edu.au (B. Hoex), zghuang@jou.edu.cn (Z. Huang).
[1] Ying Liu and Borong Sang contributed equally to this work.

https://doi.org/10.1016/j.solener.2021.09.083
Received 11 August 2021; Received in revised form 26 September 2021; Accepted 29 September 2021
Available online 6 October 2021

efficiency of 23.1% using a $TiO_x/LiF_x/Al$ layer stack. Meanwhile, TiO_x thin films have shown good passivation at the c-Si/TiO_x interface, which is probably attributed to the negative fixed charge at the interface or the chemical passivation effect (Liao et al., 2013; Sahasrabudhe et al., 2015). However, there is still no comprehensive understanding of the TiO_x passivation mechanism (Melskens et al., 2018). With its ultimate control of the process, ALD is an appealing method to deposit thin films of high quality and conformity at low substrate temperatures (typically around 150 °C) (Hossain et al., 2020). Liao et al. (2013) were the first to report excellent passivation of the c-Si surface by TiO_2 films grown using ALD. The key was to ensure sufficiently low substrate temperature during deposition so that the TiO_2 films remained amorphous. In addition, they showed that the surface passivation significantly improved after light soaking, very likely attributed to the trapping of charge in bulk defects in the TiO_2 film, which improved surface passivation by charge carrier control. Yang et al. (2016a) obtained an effective minority carrier lifetime of 850 μs and calculated surface recombination velocity of 11 $cm{\cdot}s^{-1}$ using a 5.5 nm ALD-TiO_2 passivation film annealed at 250 °C for silicon, while the surface passivation degraded with a higher annealing temperature. However, the simultaneous achievement of excellent conductivity and passivation of TiO_2 thin film is yet not satisfied. Yang et al. (2016b) reported an effective minority carrier lifetime (τ_{eff}) of 865 μs and a contact resistivity (ρ_c) value of 0.75 $\Omega{\cdot}cm^2$ for a 5.5 nm ALD-TiO_x films, and a relatively low ρ_c value of 0.25 $\Omega{\cdot}cm^2$ was obtained for 4.5 nm TiO_x film.

An appealing way to alter the properties of semiconductors is the introduction of dopants that can change material properties such as bandgap, work function, charge carrier recombination rates and conductivity (Kösemen et al., 2016; Mogal et al., 2013). First-principles density functional (DFT) and experimental studies revealed that substitutional fluorine (F) dopants at the oxygen sites resulting in moving the Fermi level close to the conduction band (CB) of TiO_2, and thus, increasing its conductivity and favouring better electron transport in contact with *n*-type c-Si (He et al., 2019). Currently, doping of TMOs has already been successfully used to improve the performance of organic and perovskite solar cells and water-splitting devices (Altomare et al., 2013; Lü et al., 2010; Wang et al., 2015; Wu et al., 2016). However, limited work has been reported for improving passivating contacts for c-Si using doped TiO_2.

In this work, we start with DFT to identify dopants for TiO_2 that improve the electron conductivity. Subsequently, we use the ALD supercycle technique to grow Al-doped TiO_2 (ATO). We study the structural properties and elemental composition of the ALD-ATO films by Transmission Electron Microscope (TEM), X-ray photoelectron spectra (XPS), and time-of-flight secondary ion mass spectrometry (ToF-SIMS). By controlling the ratio of Al: Ti, excellent passivation (τ_{eff} of 1.9 ms) and conductivity (ρ_c of 0.1 $\Omega{\cdot}cm^2$) of ALD-ATO films were simultaneously achieved, which are significantly better compared to intrinsic TiO_2 films. Also, ALD-ATO films show higher thermal stability compared to intrinsic TiO_2. Finally, the most promising ATO film was applied on the illumined side of a passivated emitter and rear contact (PERC) solar cell (118.7 × 100 mm^2) and a champion efficiency of 21.4% was obtained.

2. Experimental Section

2.1. ALD-ATO films deposition and device fabrication

Before ATO deposition, N-type (1 0 0)-oriented zone silicon wafers (~285 μm, ~3 Ω·cm) were chemical-polished, RCA 1 & 2 (Kern and Puotinen, 1970) cleaned followed by an HF (2%) dip. Native grown SiO_2 was then removed using an HF dip, followed by a chemically grown thin SiO_2 by RCA2. ATO films with a cycle ratio (Al: Ti): 1:5, 1:30, 1:60, 1:120 were deposited by ALD at a substrate temperature of 150 °C with the trimethyl-aluminium (TMA), titanium tetrakis (dimethylamide) (TDMAT) and H_2O as the precursors. For the lifetime measurement samples, the ATO was deposited on both sides of the wafer. For the TLM measurements, the ATO film was grown on one side of the c-Si wafer. The growth per cycle was ~0.69 Å. For cycle ratio (Al: Ti) = 1:5, 1 cycle Al_2O_3 film was deposited following 5 cycles TiO_2 films, where such a whole cycle is called a supercycle, as shown in Fig. S1. 40 supercycles were deposited to achieve a total of 240 ALD cycles. Each ratio has a slight difference, and the values of cycles with the ratio of 1:5, 1:30, 1:60 and 1:120 are 240, 248, 183 and 242. The samples were annealed at 250 °C, 300 °C and 350 °C for 15 min, respectively, In nitrogen (N_2) ambient to explore the effect of the annealing temperature on the ATO films. The annealing process was done in a rapid thermal processing (RTP) system (ECM Jetfirst).

PERC cells with ATO or undoped TiO_2 films were fabricated on p-type c-Si wafers (≈175 μm, 2.0 Ω·cm). The cell area (118.7 × 100 mm^2) was then realized by photolithographically defined mesa etch. The stack SiO_2/ATO or undoped TiO_2 (60 ALD cycles)/SiN_x (PECVD) layers was used to passivate the n^+ emitter. The rear reflector consists of stack Al_2O_3 (ALD)/SiN_x (PECVD) layers and screen-printed Al. All the PERC cells were fired in the industrial sintering furnace (CF-Series, Despatch) at the peak temperature of 800 °C.

2.2. Modelling

The first-principles DFT calculations were carried out using the projector augmented wave (PAW) pseudopotentials as implemented in the Vienna Ab-initio Simulation Package (VASP). The electron interactions were first described by the generalized gradient approximation (GGA) as formulated in the Perdew-Burke-Ernzerhof (PBE) functional and a plane wave basis set with a kinetic energy cutoff of 500 eV. The Brillouin zone for the 2 × 2 × 3 TiO_2 supercell (144 atoms) was integrated using a 3 × 3 × 1 Monkhorst-Pack generated *k*-point mesh and Gaussian smearing of 0.01 eV. Then the selected calculations were repeated with the hybrid functional of Heyd–Scuseria–Ernzerhof (HSE06). Tight convergence criteria for ionic and electronic of 1×10^{-6} and 1×10^{-7} eV, respectively, were set optimize total orbital energies which resulted in a converged total energy of < 1 meV. The volume, shape and atomic positions were considered for structural relaxation until the residual force becomes <0.01 eV/Å in the supercell, and spin-polarized electronic density of states (DOS) was computed using the tetrahedron scheme.

2.3. Characterization

The TEM sample structure was Pt/ATO/SiO_2/n-Si (100 nm/16.5 nm/1.5 nm/~285 μm), where Pt film was thermally evaporated on a wafer with a single side ATO film deposition, ATO film with cycle ratio Al: Ti = 1:5, after 300 °C annealing in N_2-gas for 15 min, for transmission electron microscopy (TEM, FEI Talos) coupled with energy-dispersive X-ray spectroscopy (EDS). The time-of-flight secondary ion mass spectrometry (ToF-SIMS, IONTOF) was utilized to determine the element depth and X-ray photoelectron spectroscopy (XPS) (ESCALAB250Xi Thermo Scientific, UK) was employed to examine the elemental composition at the surface under ultrahigh vacuum (pressure below 2×10^{-9} mbar). The X-ray source was monochromatic Al Kα ($h\nu = 1486.68$ eV) calibrated using the carbon reference. ATO films were fabricated on an oxide-covered silicon wafer. To measure the level of surface passivation, the symmetrically coated sample was measured before and after annealing by quasi-steady-state photoconductance (QSSPC) using a Sinton Instruments WCT120 photoconductance tester and the lifetimes were recorded at an excess minority carrier density of 1×10^{15} cm^{-3}. The contact resistivity was extracted using the transfer-length method (TLM). The width of electrode of the TLM pattern is 3 mm and the pad spacing is 0.15, 0.2, 0.3, 0.4, 0.6 and 0.8 mm, respectively. A LiF/Al (~1 nm/100 nm) stacks were thermally evaporated via a shadow mask on the ATO film before the contact resistance measurements. The dark current-voltage (I-V) measurements were performed after annealing

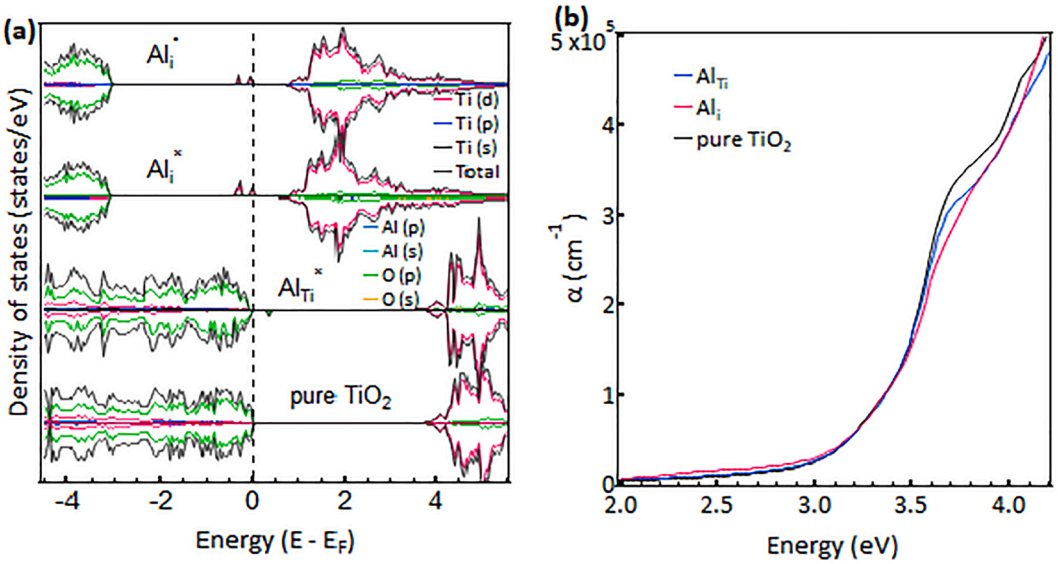

Fig. 1. (a) Hybrid density functional theory (DFT) calculated spin-polarized total and species-projected DOS plots of pristine TiO_2 as well as substitutional and interstitial Al-doped TiO_2 in their neutral and charged states of $Al_{Ti}^{\times}$, $Al_i^{\times}$, andAl_i. (b) DFT calculated optical absorption spectra of TiO_2 with substitutional and interstitial Al dopant. The absorption spectra of pristine TiO_2 is also shown as a reference.

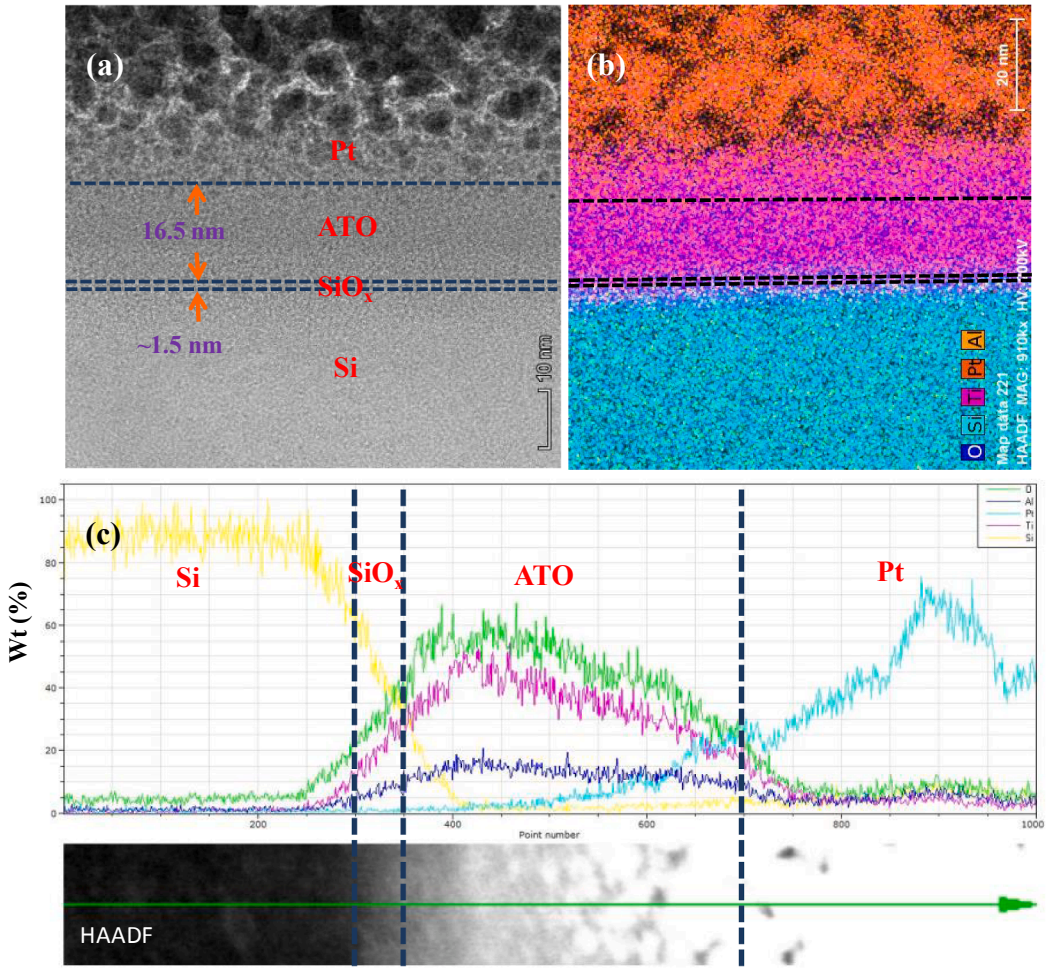

Fig. 2. (a) Cross-sectional TEM image; (b) EDS element mapping (Si, Ti, Al, O and Pt); (c) HAADF-STEM microscopy images alongside EDS line scan of a c-Si/SiO_x/ ATO (Al:Ti = 1:5) /Pt interface.

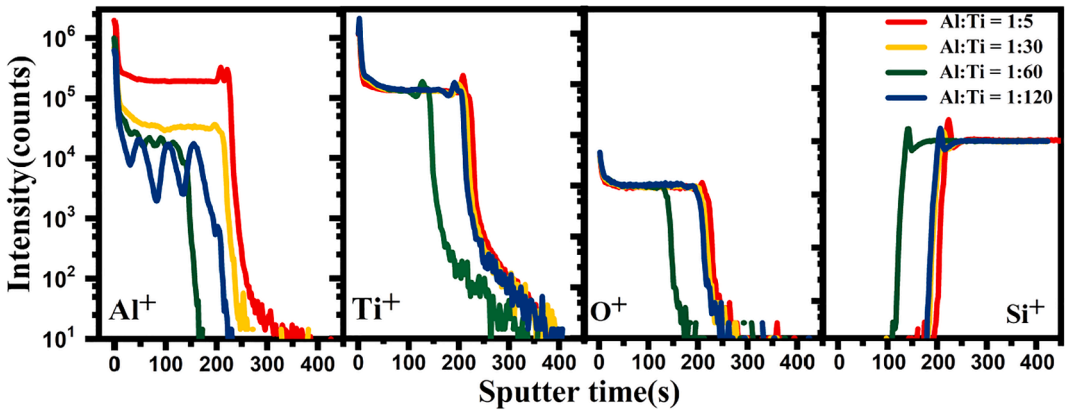

Fig. 3. ToF-SIMS depth profile of ATO films which were grown using different ALD supercycle ratios. The composition profiles of Al, Ti, O, and Si are shown.

according to pad spacing using a Keithley 2400 source meter. The contact resistivity was obtained by fitting the curve of resistance versus pad spacing. The optical data was collected by a spectral ellipsometer (SE) system (J.A. Woollam M-2000) in the 300–1000 nm wavelength range at a fixed incident angle of 70°. The optical constants of the layers were fitted with a Cody–Lorentz oscillator.

The photoluminescence photos were taken by a PL imaging analysis system (LIS-R2, BTimaging). The reflectance spectra, as well as the IQEs and EQEs, were measured on the platform of quantum efficiency measurement (QEX10, PV Measurements). The current-voltage (I-V) characteristics of the solar cells were investigated under the illumination of AM1.5 (Crown Tech IVTest Station 2000). The cell efficiency was measured using a BERGER Lichttechnik Single Cell Tester.

3. Results and discussion

3.1. Modelling of Al-doped anatase TiO_2 with DFT

Fig. 1(a) shows the spin-resolved partial and total density of states (DOS) plots of substitutional $(Al_{Ti}^{\times})$ and interstitial $(Al_i^{\times})$ Al-doped anatase TiO_2 obtained from hybrid (HSE06) DFT calculations. The plot clearly shows defect energy levels localizes close to the valence band maximum (VBM) for the $Al_{Ti}^{\times}$ as well as close to the conduction band minimum (CBM) for the $Al_i^{\times}$ and Al_i defects of the TiO_2. The charge-neutral $Al_{Ti}^{\times}$ creates defect states close to VBM, which is unfavourable for the n-type conductivity of TiO_2. However, both the charge-neutral and singly charged $Al_i^{\times}$ and Al_i create defect states close to the conduction band and narrow down the bandgap which would increase the n-type conductivity of TiO_2. These shallow defect states play an important role in charge carrier transport via these states from the c-Si to contact. The orbital-resolved projected DOS confirms that these defects states are originated from the Ti 3d and O 2p orbitals. Titanium interstitial (Ti_i) is known to improve the transport properties of TiO_2 (Li et al., 2015). The DFT calculated formation energy 6.0 eV of $Al_i^{\times}$ is lower than that of 8.1 eV for the $Ti_i^{\times}$ confirming that additional electrons from the $Al_i^{\times}$ results in more Ti^{3+} into TiO_2, which directly improves the electron transport properties.

In addition to the electronic properties, the optical properties are also crucial to reduce parasitic absorption in solar cells. While a pristine TiO_2 is transparent to visible light, it can absorb visible light due to the defect states, i.e., reduced Ti^{3+} states. The DFT calculated absorption spectra shown in Fig. 1(b) reveals that both $Al_{Ti}^{\times}$ and $Al_i^{\times}$ defects do not substantially change the optical response of TiO_2.

3.2. Characterization of ATO thin films

To investigate the structure of the ATO thin films, stack layers of c-Si/SiO_x/ATO/Pt were prepared. The elemental composition of the ATO films was determined by transmission electron microscope (TEM), energy-dispersive X-ray spectroscopy (EDS) mapping and EDS line scan. Fig. 2(a) shows the cross-sectional TEM image of a c-Si/SiO_x/ATO(Al:Ti = 1:5)/Pt sample where the ATO film was grown with an ALD

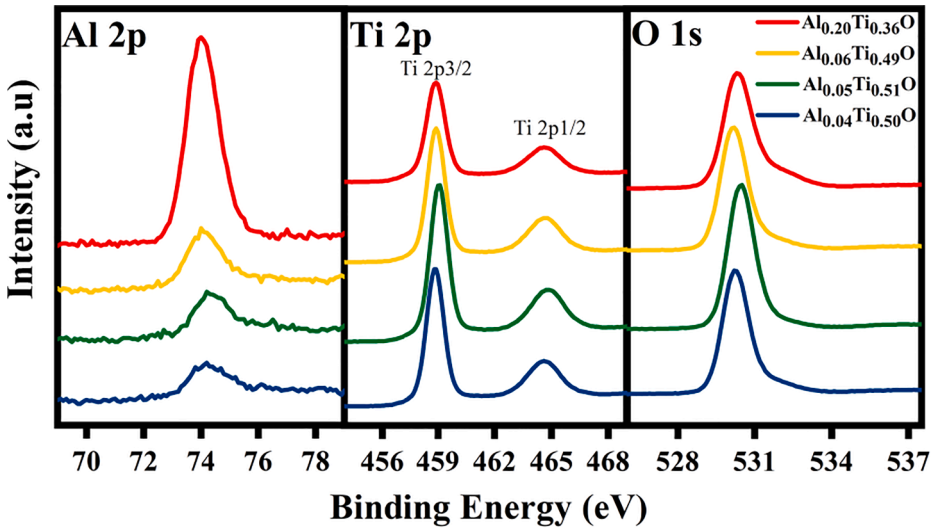

Fig. 4. XPS spectra of Al 2p, Ti 2p and O 1s for the ALD Al_xTi_yO films. The spectra were offset vertically for clarity.

Table 1
XPS binding energies and atomic ratios of Al, Ti and O in the four ALD ATO films.

Cycle ratio	Atomic %			Peak BE				Normalized
(Al: Ti)	Al 2p	Ti 2p	O 1s	Al 2p	Ti $2p_{3/2}$	Ti $2p_{1/2}$	O 1s	formula
1:5	10.8	20.2	55.3	74.0	458.8	464.5	530.3	$Al_{0.20}Ti_{0.36}O$
1:30	3.5	27.2	55.8	74.1	458.8	464.5	530.2	$Al_{0.06}Ti_{0.49}O$
1:60	2.9	30.6	59.5	74.4	458.9	464.6	530.5	$Al_{0.05}Ti_{0.51}O$
1:120	2.4	27.6	55.4	74.2	458.7	464.4	530.2	$Al_{0.04}Ti_{0.50}O$

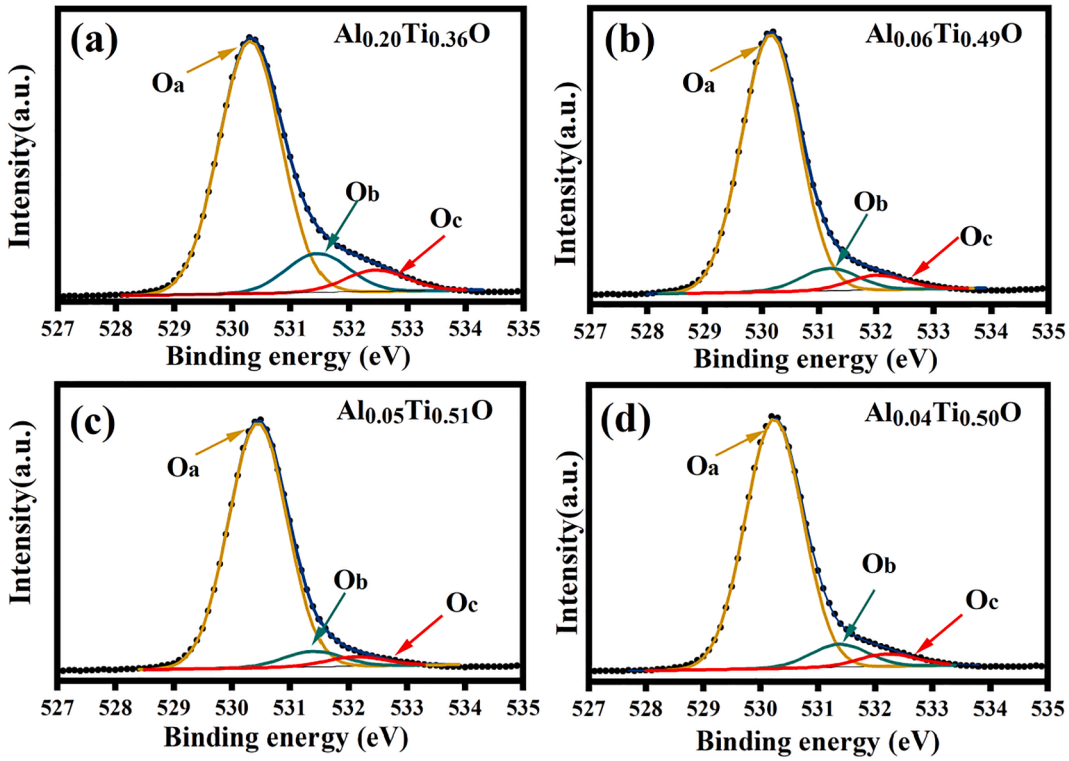

Fig. 5. Deconvoluted XPS O1s spectra of (a) $Al_{0.20}Ti_{0.36}O$, (b) $Al_{0.06}Ti_{0.49}O$, (c) $Al_{0.05}Ti_{0.51}O$, and (d) $Al_{0.04}Ti_{0.50}O$.

supercycle ratio of Al: Ti = 1:5 and annealed at 300 °C in N_2-gas for 15 min. The ATO film was grown using 240 ALD cycles, resulting in a thickness of 16.5 nm, indicating a growth per cycle (GPC) of 0.69 Å. A SiO_x interlayer (~1.5 nm) between c-Si and the ATO can clearly be observed. The c-Si/SiO_x/ATO/Pt interface was further analyzed using EDS elemental mapping to confirm the composition of these layers in Fig. 2(b), which clearly shows the presence of a SiO_x/ATO interlayer between c-Si and Pt layer and uniform distribution of both Al and Ti in the ATO layer. Meanwhile, high angle annular dark-field (HAADF) scanning TEM coupled with EDS line scan is also used to determine the atomic composition (Fig. 2(c)). The HAADF measurements corroborate the EDS results and indicate the presence of the SiO_x interface layer and a uniform ATO layer.

The annealed ATO films at 300 °C are also analyzed with ToF-SIMS and XPS to determine the atomic depth profile and chemical composition (Figs. 3 and 4). The presence of Al concentrations is clearly changed with different Al: Ti ratios in the ALD-ATO films. Fig. 3 shows that the distribution of Al was relatively uniform for ATO films grown using 1:5 and 1:30 ALD cycle ratios. At the same time, the Al concentration was not constant for higher ALD cycle ratios of 1:60 and 1:120, which is to be expected. The Al^+, Ti^+, and O^+ signals constituting the coatings are rapidly dropping and, meanwhile, the Si^+ signal from the substrate material are increasing, which is consistent with the TEM results.

The doping ratios of the ATO films obtained from XPS are listed in Table 1. The atomic ratio of Al is much higher than the cycle ratio of their oxides which may be attributed to the growth rate of Al_2O_3 being higher than that of TiO_2. The atomic content ratios of Ti with the doping ratio of $Al_{0.20}Ti_{0.36}O$, $Al_{0.06}Ti_{0.49}O$, $Al_{0.05}Ti_{0.51}O$ and $Al_{0.04}Ti_{0.50}O$ are 23.4%, 31.6%, 32.7% and 32.5%. The Ti content of $Al_{0.20}Ti_{0.36}O$ is significantly less than other ratios which may because Al prefers to occupy the interstitial site rather than substitute the Ti when the Al concentration is low. When the Al concentration is high, interstitial site and substitute may exist at the same time.

Fig. 4 shows the XPS Al 2p, Ti 2p and O 1s spectra for the ATO films. The binding energy values of Al 2p were fitted by the peak at 74.2 ± 0.2 eV corresponding to the Al-O bond for the ATO films in Fig. 4a (Liou et al., 2013). In all ATO films, the typical peak located at 74.7 eV corresponding to the Al-O bond of the stoichiometric Al_2O_3 was not found, which indicates that no Al_2O_3 clusters were formed during the ALD growth (Li et al., 2017). The Ti $2p_{3/2}$ and Ti $2p_{1/2}$ feature peaks were positioned at binding energies of 458.8 ± 0.1 and 464.5 ± 0.1 eV, with all peak separations of around 5.7 eV between the two peaks (Güzelçimen et al., 2020), which means that Ti maintains a 4^+ oxidation state after the Al doping (Bronneberg et al., 2017; Reddy et al., 2013).

As depicted in Fig. 5, 3 peaks are found in deconvoluted O 1s core-level XPS spectra with binding energies at 530.3 ± 0.2 eV (Oa), 531.3 ± 0.2 eV (Ob), and 532.3 ± 0.2 eV (Oc). The Oa peaks represent the Al-O and Ti-O bonds (Liou et al., 2013; Pathak et al., 2014), the Ob peaks were associated with oxygen ions for oxygen-deficient regions which can be related to oxygen vacancies (Awan et al., 2013; Liou et al., 2013),

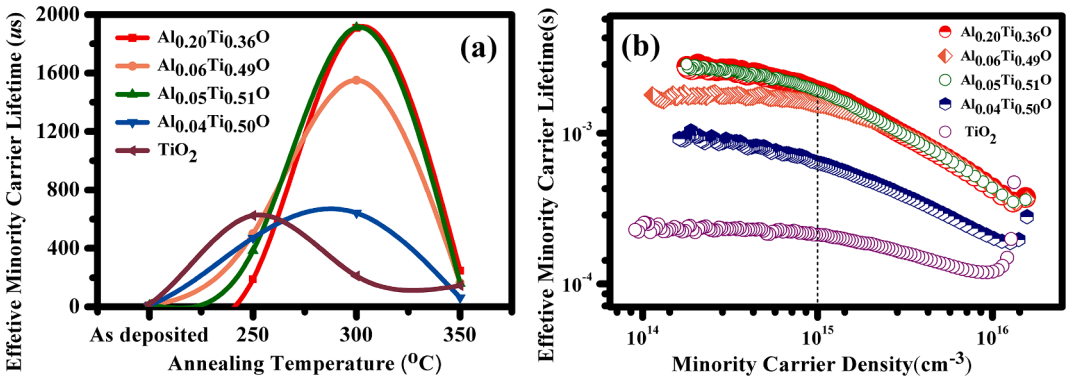

Fig. 6. (a) Effective minority carrier lifetime at an injection level of 10^{15} cm^{-3} as a function of the annealing temperature for c-Si samples symmetrically coated with ATO films with various Al:Ti ratios. (b) Injection-level-dependent effective minority carrier lifetimes of n-type c-Si wafers symmetrically passivated by various ATO films after 300°C annealing.

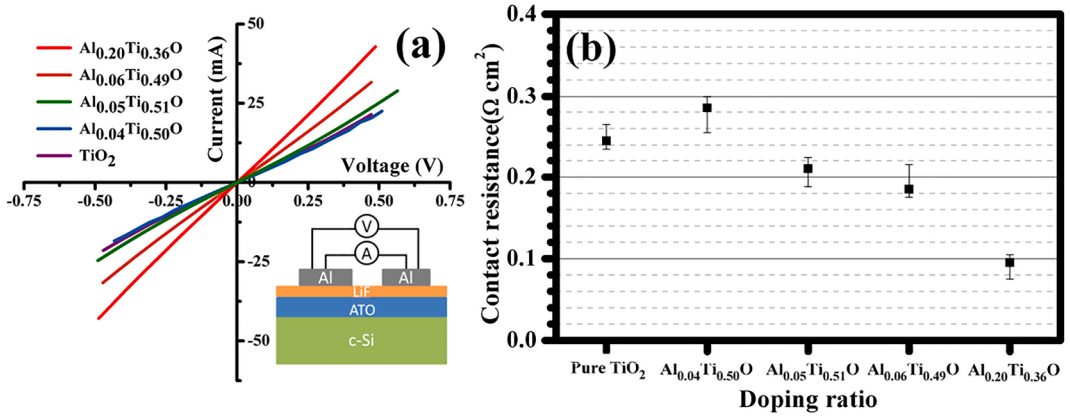

Fig. 7. (a) TLM measurement set up schematic and I-V measurement results for undoped TiO_2 and various ATO films. (b) Contact resistance for undoped TiO_2 and various ATO films on c-Si as determined by TLM.

and the Oc peaks were attributed to hydroxyl (—OH) due to H_2O in ALD or water absorbed at the surface. It was observed that the ATO film with the highest Al concentration had the highest density of oxygen vacancies (Fig. 5(a)). It is believed that the oxygen vacancies are created when Al atoms are doped into TiO_2, resulting in free electrons in the film (Said et al., 2017; Wu et al., 2012). Besides, during the ALD process, hydrogen from the precursor can also consume the oxygen in the TiO_2 layer (Pan et al., 2013). Such a higher density of oxygen vacancies and increased electrons concentration contribute to higher conductivity of ALD-ATO films with a higher Al concentration (Yi et al., 2018), where the result is consistent with the DFT calculation and the measurement of conductivity to be discussed in detail below.

3.3. Passivation and conductivity properties

The minority carrier lifetime of c-Si wafers, symmetrically coated with ~16.5 nm ATO films containing different Al doping levels, was measured to quantify the level of c-Si surface passivation provided by ATO. As shown in Fig. 6(a), the sample symmetrically passivated with an undoped TiO_2 film reaches the highest effective minority carrier lifetime after annealing at 250 °C, while the lifetime reduced when the sample was annealed at higher temperatures. This is most likely resulting from a phase change in the TiO_2 film (Liao et al., 2014; Yang et al., 2016a). However, when the TiO_2 was doped with Al, the sample can clearly tolerate higher annealing temperatures up to 300 °C, indicating increased thermal stability to ~300 °C. At a higher annealing temperature of 350 °C, the effective lifetime drops again, which could be caused by a phase change in the material. The incorporation of impurities, such as Al limits the shift of lattice and movement of dislocation; thus, inhibiting the crystallization process which is known to be beneficial for passivation of the c-Si surface. A champion effective minority carrier lifetime of 1.9 ms at an injection level of 1×10^{15} cm^{-3} was achieved using the symmetrically coated c-Si with an $Al_{0.05}Ti_{0.51}O$ film (1:60 cycle ratio) and after annealing at 300°C. This corresponded to an implied voltage of 688 mV and a recombination current density of 38 $fA{\cdot}cm^{-2}$ as shown in Fig. 6(b) and Fig. S2. Consequently, the introduction of Al into TiO_x was found to improve surface passivation and the thermal stability of the film.

Improving the conductivity of ATO thin layer is crucial to enhance performance as a passivating contact with c-Si. Consequently, transmission line measurements (TLM) were used to determine the conductivity of the material, and the results are shown in Fig. 7. A very thin layer of LiF was deposited on the top of ~16.5 nm ATO layer to enhance the charge transport following the work of He et al. (2019). As shown in Fig. 7(a), the I-V measurements for the same films indicates that all the contacts showed an Ohmic behavior. According to Fig. 7(b), the contact resistance was found to decrease as a function of the Al concentration, and a lowest contact resistance of 0.1 $\Omega{\cdot}cm^2$ is found in $Al_{0.20}Ti_{0.36}O$ sample which has the highest Al concentration among the tested samples. The downward trend of contacts resistance with an increased Al concentration is consistent with the DFT simulation results where interstitial Al-doped TiO_2 creates defect states close to the CBM; thus, increases the conductivity. The incorporation of interstitial Al is expected to move the Fermi level towards the CBM, inducing band bending at the interface of Si. The bend bending thus reduces the conduction band offset between ATO and Si, which will increase the electron

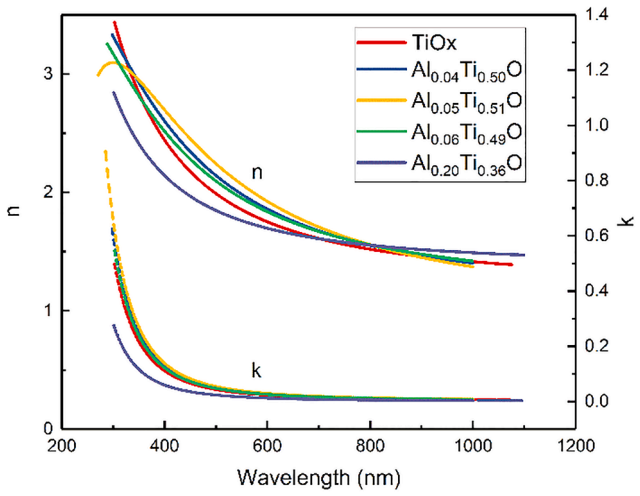

Fig. 8. The refractive index (n) and extinction coefficient (k) of ATO films with different Al: Ti ratios ATOs as determined from spectroscopic ellipsometry measurements.

selectivity and consequently reduce the film conductivity (Yang et al., 2016a). It should be noted that for very high Al concentrations, the film would become resistive as Al_2O_3 is an insulator with a relatively high bandgap. However, for relatively low Al concentrations, Al acts as a dopant resulting in an improved conductance.

3.4. Optical properties

It is worthwhile to investigate the optical properties of the film to see the impact of Al incorporation. The refractive index (n) and extinction coefficient (k) were determined from the fitting of the spectroscopic ellipsometry data (Fig. 8). ATO films with different Al: Ti ratio have shown quite similar k values with that of the pure TiO_2 film throughout the wavelength range of 300–1100 nm, suggesting that the film optical properties were not heavily affected by doping, which further supports the DFT calculated optical absorption spectra as shown in Fig. 1(b). All films also had a very similar n value which is quite close to the optimal value for an antireflection coating on silicon in a PV module. Combined with a low parasitic absorption loss, the ATO is an appealing candidate for application on the front of a solar cell.

3.5. Solar cells

As a proof of principle, the optimal ATO films were applied on the illumined side of *p*-type PERC (Zhao et al., 1999) solar cells (118.7 × 100 mm^2, more details of the design are given in the Experimental). A photograph of the solar cell is shown in Fig. 9(f), and the schematic of the device structure is shown in Fig. 9(b).

Fig. 9(a) shows the internal quantum efficiencies (IQE) and front surface reflection of the PERC solar cells with an undoped TiO_2 and $Al_{0.20}Ti_{0.36}O$ film. The cell with $Al_{0.20}Ti_{0.36}O$ film shows a slightly lower reflectance in the wavelength of 300–370 nm and a higher IQE and EQE across the 300–500 nm range than that with undoped TiO_2 as shown in Fig. 9(a) and (c). The increase in IQE was attributed to better surface passivation provided by the ATO film compared to the undoped TiO_2 film. This also demonstrates that the ATO layer still provides surface

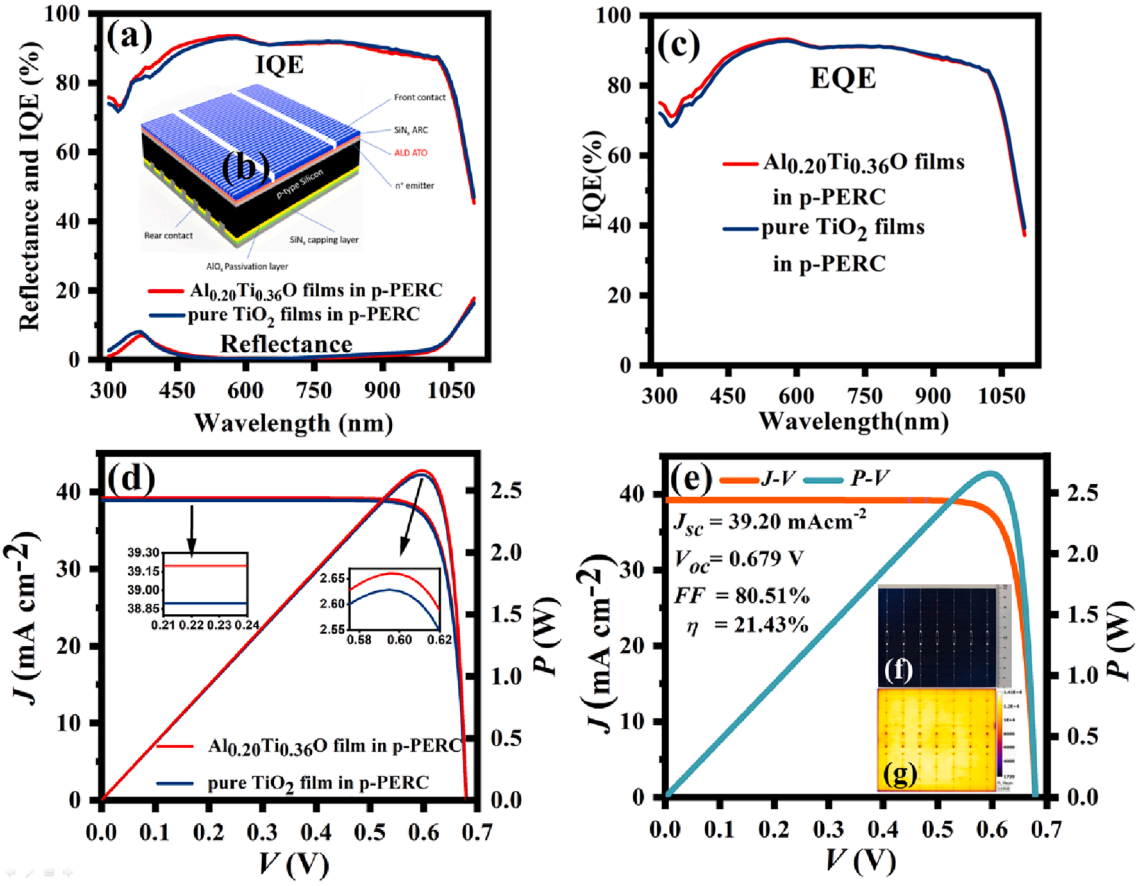

Fig. 9. (a) The EQE, Reflectance, (b) The schematic, (c) IQE, (d) *J-V* and *P-V* curve of the PERC solar cell with an $Al_{0.20}Ti_{0.36}O$ or TiO_2 film. (e) The *J-V* and *P-V* curve, (f) photograph and (g) PL images of the champion solar cell with a 21.4% efficiency featuring an $Al_{0.20}Ti_{0.36}O$ film.

Table 2
Output performances of PERC with ATO and pure TiO_2 films.

Cell (118.7×100 mm^2)		Output parameters				
		J_{sc}	V_{oc}	R_s	FF	η
		mA·cm^{-2}	V	Ω	%	%
$Al_{0.20}Ti_{0.36}O$	Average	39.22	0.677	4.078E−03	80.56	21.34
	Best	39.20	0.679	3.888E−03	80.51	21.43
TiO_2	Average	38.86	0.674	4.230E−03	80.37	21.04
	Best	38.90	0.677	4.324E−03	80.20	21.13

passivation after a short high temperature firing step. The improvement of the EQE and IQE can be attributed to the lower absorption of ATO compared to undoped TiO_x, as discussed in Section 3.4. Therefore, the solar cell with $Al_{0.20}Ti_{0.36}O$ film has a better performance compared to its undoped TiO_2 counterpart, which is further confirmed by the current density–voltage (*J-V*) and power-voltage (*P-V*) curves of devices (Fig. 9 (d)).

The *J-V* and *P-V* curves of the champion cell are shown in Fig. 9(e). The champion cell reached a η of 21.43% with an open-circuit voltage (V_{oc}) of 0.679 V, short-circuit current density (J_{sc}) of 39.20 mA·cm^{-2}, fill factor (*FF*) of 80.51%, and series resistance (R_s) of 3.888 mΩ. The peak power of the champion cell is up to 2.544 W (118.7×100 mm^2). The photoluminescence (PL) image in Fig. 9 (g) shows uniform surface passivation which is an important factor to obtain a high η of the solar cell. Table 2 shows the output performances of the fabricated devices. The average V_{oc} (0.677 V) of the solar cells with the $Al_{0.20}Ti_{0.36}O$ films was higher than the solar cell with an undoped TiO_2 film due to a higher level of surface passivation. Importantly, the average R_s (4.078 mΩ) of the solar cells with the $Al_{0.20}Ti_{0.36}O$ film was lower than that of the undoped TiO_2, attributing to the better CSC performance of the ATO film. Finally, benefiting from the excellent passivation and conductivity of ATO layers, the highest η of 21.43% of PERC solar cell with ATO is successfully achieved.

4. Conclusions

In summary, guided by DFT calculation, we systematically investigate the structure, analysis of elements, passivation, conductivity and optical property of ATO thin films. By employing the controllable ALD-Al doping technique, we successfully achieve the simultaneous improvement of passivation and conductivity of ATO thin films. For the $Al_{0.20}Ti_{0.36}O$ thin film, we obtain the highest minority carriers lifetime of 1.9 ms and the lowest contact resistivity of 0.1 Ω·cm^2 in the condition of 300°C and N_2 ambient annealing. Also, we find that the low absorption of ATO thin film makes it an appealing candidate for application on the front of a solar cell. Based on the superiorities of ATO thin films, we successfully apply the optimal ATO film on the illumined side of p-type PERC solar cells (118.7×100 mm^2) and obtain that the solar cell with ATO film has a better performance compared to its undoped TiO_2 counterpart because of the higher passivation and lower parasitic light absorption of ATO film. Furthermore, the lower average R_s of the solar cells with ATO reveals that ATO film possesses better performance of CSC for PERC solar cell. Finally, benefiting from the excellent passivation and well conductivity of ATO stack layers, we achieve a champion solar cell η of 21.4%, as well as V_{oc} of 679.1 mV, J_{sc} of 39.2 mA·cm^{-2}, and *FF* of 80.5%. The novel ALD-ATO thin-film demonstrates great potentials as passivating contacts for the high-efficiency crystalline silicon solar cells.

Declaration of Competing Interest

The authors declare that they have no known competing financial interests or personal relationships that could have appeared to influence the work reported in this paper.

Acknowledgments

This work was supported by the Natural Science Foundation of China (61774069, 11834011, 11974242 and 62034009), the Major projects of the Natural Science Foundation of universities in Jiangsu Province (20KJA430013), the “333” Project of Jiangsu Province, the “Qinglan” Project of Jiangsu Education Department, the Natural Science Foundation of Jiangsu Province (BK20201027), the Postgraduate Research & Practice Innovation Program of Jiangsu Province (KYCX20_2930, KYCX21_3139), Lianyungang Haiyan Plan (2020-QD-010), ARENA as part of ARENA’s Research and Development Program–Solar PV Research (Grant No. 2017/RND007). The HPC resources were provided by the National Computational Infrastructure (NCI), which is supported by the Australian Government, and through the UNSW-NCI partner trial scheme. The views expressed herein are not necessarily the views of the Australian Government, and the Australian Government does not accept responsibility for any information or advice contained herein.

Appendix A. Supplementary material

Supplementary data to this article can be found online at https://doi.org/10.1016/j.solener.2021.09.083.

References

Altomare, M., Lee, K., Killian, M.S., Selli, E., Schmuki, P., 2013. Ta-doped TiO_2 nanotubes for enhanced solar-light photoelectrochemical water splitting. Chem. - A Eur. J. 19, 5841–5844. https://doi.org/10.1002/chem.201203544.

Awan, S.U., Hasanain, S.K., Bertino, M.F., Jaffari, G.H., 2013. Effects of substitutional Li on the ferromagnetic response of Li co-doped ZnO: Co nanoparticles. J. Phys. Condens. Matter 25, 156005. https://doi.org/10.1088/0953-8984/25/15/156005.

Bronneberg, A.C., Höhn, C., Van De Krol, R., 2017. Probing the interfacial chemistry of ultra-thin ALD-grown TiO_2 films: an in-line XPS study. J. Phys. Chem. C 121, 5531–5538. https://doi.org/10.1021/acs.jpcc.6b09468.

Bullock, J., Wan, Y., Hettick, M., Zhaoran, X., Phang, S.P., Yan, D., Wang, H., Ji, W., Samundsett, C., Hameiri, Z., Macdonald, D., Cuevas, A., Javey, A., 2019. Dopant-free partial rear contacts enabling 23% silicon solar cells. Adv. Energy Mater. 9, 1–6. https://doi.org/10.1002/aenm.201803367.

Feldmann, F., Bivour, M., Reichel, C., Hermle, M., Glunz, S.W., 2014. Passivated rear contacts for high-efficiency n-type Si solar cells providing high interface passivation quality and excellent transport characteristics. Sol. Energy Mater. Sol. Cells 120, 270–274. https://doi.org/10.1016/j.solmat.2013.09.017.

Güzelçimen, F., Tanören, B., Çetinkaya, Ç., Kaya, M.D., Efkere, H.İ., Özen, Y., Bingöl, D., Sirkeci, M., Kınacı, B., Ünlü, M.B., Özçelik, S., 2020. The effect of thickness on surface structure of rf sputtered TiO_2 thin films by XPS, SEM/EDS, AFM and SAM. Vacuum 182. https://doi.org/10.1016/j.vacuum.2020.109766.

He, J., Hossain, M.A., Lin, H., Wang, W., Karuturi, S.K., Hoex, B., Ye, J., Gao, P., Bullock, J., Wan, Y., 2019. 15% Efficiency Ultrathin Silicon Solar Cells with Fluorine-Doped Titanium Oxide and Chemically Tailored Poly(3,4-ethylenedioxythiophene):Poly(styrenesulfonate) as Asymmetric Heterocontact. ACS Nano 13, 6356–6362. https://doi.org/10.1021/acsnano.9b01754.

Hossain, M.A., Khoo, K.T., Cui, X., Poduval, G.K., Zhang, T., Li, X., Li, W.M., Hoex, B., 2020. Atomic layer deposition enabling higher efficiency solar cells: A review. Nano Mater. Sci. 2, 204–226. https://doi.org/10.1016/j.nanoms.2019.10.001.

Kern, W., Puotinen, D.A., 1970. Cleaning solution based on hydrogen peroxide for use in silicon semiconductor technology. RCA Rev. 31, 187–206. https://doi.org/10.1029/RS005i012p01489.

Kösemen, A., Alpaslan Kösemen, Z., Canimkubey, B., Erkovan, M., Başarir, F., San, S.E., Örnek, O., Tunç, A.V., 2016. Fe doped TiO_2 thin film as electron selective layer for inverted solar cells. Sol. Energy 132, 511–517. https://doi.org/10.1016/j.solener.2016.03.049.

Li, L., Xia, C., Li, W., Ji, A., Zhu, C., Zhang, L., Wang, Z., Yang, J., Mao, L.F., 2015. Nature of the interstitials in titanium dioxide and their impact on transmission coefficient: ab initio calculations. J. Nanomater. 2015, 574752 https://doi.org/10.1155/2015/574752.

Li, Y., Yao, R., Wang, H., Wu, Xiaoming, Wu, J., Wu, Xiaohong, Qin, W., 2017. Enhanced performance in Al-doped ZnO based transparent flexible transparent thin-film transistors due to oxygen vacancy in ZnO film with Zn-Al-O interfaces fabricated by atomic layer deposition. ACS Appl. Mater. Interfaces 9, 11711–11720. https://doi.org/10.1021/acsami.7b02609.

Liao, B., Hoex, B., Aberle, A.G., Chi, D., Bhatia, C.S., 2014. Excellent c-Si surface passivation by low-temperature atomic layer deposited titanium oxide. Appl. Phys. Lett. 104, 253903 https://doi.org/10.1063/1.4885096.

Liao, B., Stangl, R., Mueller, T., Lin, F., Bhatia, C.S., Hoex, B., 2013. The effect of light soaking on crystalline silicon surface passivation by atomic layer deposited Al_2O_3. J. Appl. Phys. 113, 024509 https://doi.org/10.1063/1.4775595.

Liou, Y.J., Chen, Y.J., Chen, B.R., Lee, L.M., Huang, C.H., 2013. XPS study of aluminum coating on TiO_2 anode of dye-sensitized solar cells. Surf. Coatings Technol. 231, 535–538. https://doi.org/10.1016/j.surfcoat.2012.02.008.

Lü, X., Mou, X., Wu, J., Zhang, D., Zhang, L., Huang, F., Xu, F., Huang, S., 2010. Improved-performance dye-sensitized solar cells using Nb-doped TiO_2 electrodes: efficient electron injection and transfer. Adv. Funct. Mater. 20, 509–515. https://doi.org/10.1002/adfm.200901292.

Matsui, T., Bivour, M., Ndione, P.F., Bonilla, R.S., Hermle, M., 2020. Origin of the tunable carrier selectivity of atomic-layer-deposited TiO_x nanolayers in crystalline silicon solar cells. Sol. Energy Mater. Sol. Cells 209, 110461. https://doi.org/10.1016/j.solmat.2020.110461.

Melskens, J., Van De Loo, B.W.H., Macco, B., Black, L.E., Smit, S., Kessels, W.M.M., 2018. Passivating contacts for crystalline silicon solar cells: from concepts and materials to prospects. IEEE J. Photovoltaics 8, 373–388. https://doi.org/10.1109/JPHOTOV.2018.2797106.

Mogal, S.I., Mishra, M., Gandhi, V.G., Tayade, R.J., 2013. Metal doped titanium dioxide: synthesis and effect of metal ions on physico-chemical and photocatalytic properties. Mater. Sci. Forum 734, 364–378. https://doi.org/10.4028/www.scientific.net/MSF.734.364.

Nagamatsu, K.A., Avasthi, S., Sahasrabudhe, G., Man, G., Jhaveri, J., Berg, A.H., Schwartz, J., Kahn, A., Wagner, S., Sturm, J.C., 2015. Titanium dioxide/silicon hole-blocking selective contact to enable double-heterojunction crystalline silicon-based solar cell. Appl. Phys. Lett. 106, 123906 https://doi.org/10.1063/1.4916540.

Pan, X., Yang, M.Q., Fu, X., Zhang, N., Xu, Y.J., 2013. Defective TiO_2 with oxygen vacancies: synthesis, properties and photocatalytic applications. Nanoscale 5, 3601–3614. https://doi.org/10.1039/c3nr00476g.

Pathak, S.K., Abate, A., Ruckdeschel, P., Roose, B., Gödel, K.C., Vaynzof, Y., Santhala, A., Watanabe, S.I., Hollman, D.J., Noel, N., Sepe, A., Wiesner, U., Friend, R., Snaith, H. J., Steiner, U., 2014. Performance and stability enhancement of dye-sensitized and perovskite solar cells by Al doping of TiO_2. Adv. Funct. Mater. 24, 6046–6055. https://doi.org/10.1002/adfm.201401658.

Reddy, K.H., Martha, S., Parida, K.M., 2013. Fabrication of novel p-BiOI/n-$ZnTiO_3$ heterojunction for degradation of rhodamine 6G under visible light irradiation. Inorg. Chem. 52, 6390–6401. https://doi.org/10.1021/ic400159m.

Sahasrabudhe, G., Rupich, S.M., Jhaveri, J., Berg, A.H., Nagamatsu, K.A., Man, G., Chabal, Y.J., Kahn, A., Wagner, S., Sturm, J.C., Schwartz, J., 2015. Low-temperature synthesis of a TiO_2/Si heterojunction. J. Am. Chem. Soc. 137, 14842–14845. https://doi.org/10.1021/jacs.5b09750.

Said, N.D.M., Sahdan, M.Z., Ahmad, A., Senain, I., Bakri, A.S., Abdullah, S.A., Rahim, M. S., 2017. Effects of Al doping on structural, morphology, electrical and optical properties of TiO_2 thin film. AIP Conf. Proc. 1788, 30130. https://doi.org/10.1063/1.4968383.

Tanaka, M., Taguchi, M., Matsuyama, T., Sawada, T., Tsuda, S., Nakano, S., Hanafusa, H., Kumano, Y., 1992. Development of new a-si/c-si heterojunction solar cells: Acj-hit (artificially constructed junction-heterojunction with intrinsic thin-layer). Jpn. J. Appl. Phys. 31, 3518–3522. https://doi.org/10.1143/JJAP.31.3518.

Tyagi, A., Ghosh, K., Kottantharayil, A., Lodha, S., 2019. An analytical model for the electrical characteristics of passivated carrier-selective contact (CSC) solar cell. IEEE Trans. Electron. Devices 66, 1377–1385. https://doi.org/10.1109/TED.2019.2893998.

Wang, J., Qin, M., Tao, H., Ke, W., Chen, Z., Wan, J., Qin, P., Xiong, L., Lei, H., Yu, H., Fang, G., 2015. Performance enhancement of perovskite solar cells with Mg-doped TiO_2 compact film as the hole-blocking layer. Appl. Phys. Lett. 106, 121104 https://doi.org/10.1063/1.4916345.

Wu, M.C., Chan, S.H., Jao, M.H., Su, W.F., 2016. Enhanced short-circuit current density of perovskite solar cells using Zn-doped TiO_2 as electron transport layer. Sol. Energy Mater. Sol. Cells 157, 447–453. https://doi.org/10.1016/j.solmat.2016.07.003.

Wu, Q., Zheng, Q., van de Krol, R., 2012. Creating oxygen vacancies as a novel strategy to form tetrahedrally coordinated Ti^{4+} in Fe/TiO_2 nanoparticles. J. Phys. Chem. C 116, 7219–7226. https://doi.org/10.1021/jp212577g.

Yang, X., Bi, Q., Ali, H., Davis, K., Schoenfeld, W.V., Weber, K., 2016a. High-Performance TiO2-based electron-selective contacts for crystalline silicon solar cells. Adv. Mater. 28, 5891–5897. https://doi.org/10.1002/adma.201600926.

Yang, X., Zheng, P., Bi, Q., Weber, K., 2016b. Silicon heterojunction solar cells with electron selective TiO_x contact. Sol. Energy Mater. Sol. Cells 150, 32–38. https://doi.org/10.1016/j.solmat.2016.01.020.

Yi, H., Wang, D., Mahmud, M.A., Haque, F., Upama, M.B., Xu, C., Duan, L., Uddin, A., 2018. Bilayer SnO_2 as electron transport layer for highly efficient perovskite solar cells. ACS Appl. Energy Mater. 1, 6027–6039. https://doi.org/10.1021/acsaem.8b01076.

Yu, J., Fu, Y., Zhu, L., Yang, Z., Yang, X., Ding, L., Zeng, Y., Yan, B., Tang, J., Gao, P., Ye, J., 2018. Heterojunction solar cells with asymmetrically carrier-selective contact structure of molybdenum-oxide/silicon/magnesium-oxide. Sol. Energy 159, 704–709. https://doi.org/10.1016/j.solener.2017.11.047.

Zhang, T., Hossain, M.A., Lee, C.Y., Zakaria, Y., Abdallah, A.A., Hoex, B., 2018. Atomic layer deposited $Zn_xNi_{1-x}O$: A thermally stable hole selective contact for silicon solar cells. Appl. Phys. Lett. 113, 262102 https://doi.org/10.1063/1.5056223.

Zhao, J., Wang, A., Green, M.A., 1999. 24.5% efficiency silicon PERT cells on MCZ substrates and 24.7% efficiency PERL cells on FZ substrates. Prog. Photovoltaics Res. Appl. 7, 471–474. https://doi.org/10.1002/(SICI)1099-159X(199911/12)7:6<471::AID-PIP298>3.0.CO;2-7.